General-Relativistic Image Rendering of a Black Hole

Author: Marta Delgado Vila, mdelgavi36@alumnes.ub.edu
Facultat de Física, Universitat de Barcelona, Diagonal 645, 08028 Barcelona, Spain.

Advisor: Raimon Luna i Perelló, raimonluna@icc.ub.edu

Abstract: We present a general-relativistic ray tracing simulation of a Schwarzschild black hole surrounded by a geometrically and optically thin accretion disk. Photon trajectories are computed by numerically integrating the null geodesic equations via a 4th-order Runge-Kutta integrator, implemented in Python with GPU parallelisation through CuPy. The resulting images reproduce the key features of the Schwarzschild spacetime: the black hole shadow, the photon ring, and the direct and lensed images of the accretion disk. Simulations are performed for various observer inclinations, illustrating how the projected morphology of the disk varies with the observation angle.
Keywords: Schwarzschild black hole, ray tracing, null geodesics, Runge-Kutta, accretion disk, gravitational lensing
SDGs: 4 (Quality Education), 9 (Industry, Innovation and Infrastructure)

I. INTRODUCTION

Einstein's field equations admit several exact solutions, each describing a distinct spacetime and type of black hole characterised by its symmetry and physical parameters. In 1916, shortly after the publication of General Relativity, Karl Schwarzschild derived the first such solution for a static, spherically symmetric spacetime. The Schwarzschild black hole is fully characterised by its mass alone, representing an uncharged, non-rotating black hole.

According to the No-Hair Theorem, any black hole is completely described by just three parameters: mass M, angular momentum J, and electric charge Q. Consistent with this, further solutions were found throughout the 20th century: the Reissner-Nordström metric (charged, non-rotating), the Kerr metric (uncharged, rotating), and the Kerr-Newman metric (charged and rotating).

The existence of black holes, long a theoretical prediction, has been confirmed by several independent lines of evidence, among them the first resolved images of black hole shadows produced by the Event Horizon Telescope (EHT) collaboration: the supermassive black hole M87* in 2019 [1], and Sagittarius A*, the black hole at the centre of the Milky Way, in 2022 [2]. Both images reveal a bright emission ring surrounding a central brightness depression, consistent with the shadow predicted by general relativity.

This thesis focuses on the Schwarzschild solution as the simplest black hole model. We implement ray tracing of the black hole surroundings by numerically integrating null geodesics with a 4th-order Runge-Kutta scheme. Although not the standard approach, this serves as a proof of concept for a generalised simulation tool.

II. THEORETICAL FRAMEWORK

A. General relativity

Special Relativity unifies space and time into a single four-dimensional continuum known as Minkowski spacetime. General Relativity extends this framework by allowing the geometry of spacetime to be dynamic: through the machinery of differential geometry, the metric tensor is no longer fixed but is determined by the distribution of energy and momentum. This dependency is expressed mathematically through the Einstein field equations (EFE),

$$R_{\mu\nu} - \frac{1}{2} g_{\mu\nu} R = \frac{8\pi G}{c^4} T_{\mu\nu}. \tag{1}$$

The curvature of spacetime forces test particles and light to follow the straightest possible paths in a curved manifold, known as geodesics. These are described by the geodesic equation,

$$\frac{d^2 x^\mu}{d\tau^2} + \Gamma^\mu_{\alpha\beta} \frac{dx^\alpha}{d\tau} \frac{dx^\beta}{d\tau} = 0. \tag{2}$$

In particular, this work makes use of null geodesics, which correspond to the trajectories of massless particles such as photons. Since the spacetime interval vanishes for photons ($ds^2 = 0$), proper time τ is not defined along their trajectories, and an affine parameter λ is used instead.

B. Schwarzschild solution

Schwarzschild's metric is a solution to Eq. (1) in vacuum ($T_{\mu\nu} = 0$) outside a spherically symmetric and static mass distribution.

Let us start by imposing spherical symmetry on a four-dimensional spacetime. Following [3], the most generic

metric in those conditions is

$$ds^2 = -e^{2\Phi(t,r)}dt^2 + e^{2\Lambda(t,r)}dr^2 + r^2 d\Omega^2. \quad (3)$$

The most appropriate coordinates for this symmetry are the Schwarzschild coordinates (t, r, θ, ϕ), and the natural choice of units are geometric units ($G = c = 1$).

Applying vacuum ($T_{\mu\nu} = 0$) and static spherical symmetry, we obtain the Schwarzschild metric,

$$ds^2 = -\left(1 - \frac{2M}{r}\right) dt^2 + \frac{dr^2}{\left(1 - \frac{2M}{r}\right)} + r^2 d\Omega^2. \quad (4)$$

This solution, published in 1916, was later proved to be the unique exterior metric for any spherically symmetric matter distribution by the Birkhoff theorem [4].

The Schwarzschild metric is a valid solution to Eq. (1) for all $r \neq 0$. At $r = 2M$, the component g_{rr} diverges, but this is a coordinate singularity rather than a physical one: it is an artifact of the Schwarzschild coordinates, and the spacetime remains perfectly regular there. In fact, we define this radius as the event horizon of the Schwarzschild black hole.

For $r < 2M$, the metric remains a valid solution, but the coordinates r and t swap their causal roles: r becomes timelike and t becomes spacelike. As a consequence, $r \to 0$ is inevitable for any infalling particle, just as the advance of time is unavoidable.

Finally, at $r = 0$ there is a genuine physical singularity, as shown in [3].

C. Effective potential

The Killing vectors of the Schwarzschild metric (Eq. (4)) are ∂_t and ∂_ϕ, which indicate the existence of two constants of motion [3],

$$u_0 = g_{00}\frac{dt}{d\tau} = -\hat{E}, \quad u_\varphi = g_{\varphi\varphi}\frac{d\varphi}{d\tau} = \hat{L} \quad (m \neq 0), \quad (5)$$

$$k_0 = g_{00}\frac{dt}{d\lambda} = -E, \quad k_\varphi = g_{\varphi\varphi}\frac{d\varphi}{d\lambda} = L \quad (m = 0). \quad (6)$$

Applying $g_{\alpha\beta}u^\alpha u^\beta = -1$ for $m \neq 0$ and $g_{\alpha\beta}k^\alpha k^\beta = 0$ for $m = 0$, and restricting to the equatorial plane $\theta = \pi/2$, without loss of generality [3], we obtain

$$\dot{r}^2 + \left(1 - \frac{2M}{r}\right)\left(1 + \frac{\hat{L}^2}{r^2}\right) = \hat{E}^2 \quad (m \neq 0), \quad (7)$$

$$\dot{r}^2 + \left(1 - \frac{2M}{r}\right)\frac{L^2}{r^2} = E^2 \quad (m = 0), \quad (8)$$

from which we identify an effective potential,

$$\hat{V}_{\text{eff}}(r) = \left(1 - \frac{2M}{r}\right)\left(1 + \frac{\hat{L}^2}{r^2}\right) \quad (m \neq 0), \quad (9)$$

$$V_{\text{eff}}(r) = \left(1 - \frac{2M}{r}\right)\frac{L^2}{r^2} \quad (m = 0). \quad (10)$$

D. Regions of a Schwarzschild black hole

Circular orbits around a spherically symmetric mass distribution are determined by $V'_{eff}(r) = 0$.

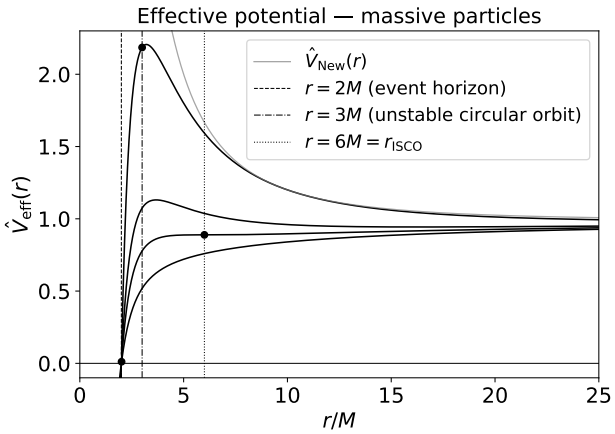

FIG. 1: $V_{\text{eff}}(r)$, for increasing values of $\hat{L}^2$ from bottom to top, for massive particles.

For massive particles, the structure of the orbits depends on $\hat{L}^2$, as shown in Fig. 1. For $\hat{L}^2 < 12M^2$ no circular orbit exists. At $\hat{L}^2 = 12M^2$ the two solutions merge into a single degenerate orbit at $r_+ = r_- = r_{\text{ISCO}} = 6M$, the innermost stable circular orbit (ISCO). For $\hat{L}^2 \gg 12M^2$, the outer stable orbit approaches $r_+ = \hat{L}^2/M$, recovering the Newtonian minimum, while the inner unstable orbit sits at $r_- = 3M$.

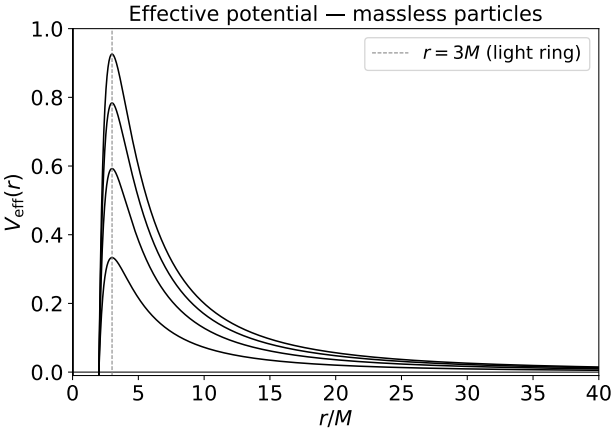

FIG. 2: $V_{\text{eff}}(r)$, for increasing values of L^2 from bottom to top. for massless particles.

For massless particles, there is only one circular orbit, located at $r = 3M$ and known as the light ring (Fig. 2). This orbit is unstable: photons with impact parameter

$b \equiv L/E$ exactly equal to the critical value

$$b_c = 3\sqrt{3}\,M \tag{11}$$

orbit indefinitely at $r = 3M$, while those with b slightly above b_c escape to infinity and those with b slightly below fall into the black hole. The critical impact parameter b_c defines the shadow radius: the apparent boundary of the black hole as seen by a distant observer.

III. METHODOLOGY

Ray tracing consists of calculating the trajectory of photons starting at the camera and propagating them towards the black hole. The trajectory is obtained by integrating Eq. (2) for each pixel, where each pixel corresponds to an independent photon. Whether a photon hits the accretion disk or escapes entirely determines the colour of each point on screen.

As previously mentioned, the integration is performed using a 4th-order Runge-Kutta (RK4) integrator. This method determines the next point in the trajectory, given the current one, by sampling the derivative of the differential equation at four strategic locations within each step: at the start, twice at the midpoint, and once at the end, combining them into a single weighted estimate. Concretely, for a differential equation of the form $dy/dx = f(x, y)$, the update at each step of size h is given by [5]

$$y_{n+1} = y_n + \frac{h}{6}(k_1 + 2k_2 + 2k_3 + k_4), \tag{12}$$

where the four derivative samples are defined as

$$k_1 = f(x_n,\, y_n), \tag{13}$$

$$k_2 = f\big(x_n + \tfrac{h}{2},\, y_n + \tfrac{h}{2}k_1\big)\,, \tag{14}$$

$$k_3 = f\big(x_n + \tfrac{h}{2},\, y_n + \tfrac{h}{2}k_2\big)\,, \tag{15}$$

$$k_4 = f(x_n + h,\, y_n + h\,k_3)\,. \tag{16}$$

The midpoint estimates k_2 and k_3 are weighted twice as heavily as the endpoint ones, since they carry more information about the behaviour of the function across the interval. This weighting is what gives RK4 its fourth-order accuracy: the error per step scales as h^5, making it significantly more precise than simpler methods for the same computational cost.

Since the geodesic equations are second-order differential equations, they are first separated into a set of coupled first-order equations, to which RK4 is then applied simultaneously. Each variable is updated together at every step, and the procedure is repeated across many small increments.

At each step, a mask, initially null, is updated to reflect whether any photons have crossed the accretion disk.

To reduce computational cost, the integration is stopped when a photon crosses the event horizon or escapes beyond a maximum radial distance.

The accretion disk is modelled as geometrically thin and optically thin, meaning it lies on the equatorial plane and allows photons to pass through it multiple times, accumulating intensity with each crossing rather than being absorbed upon first contact. The more times a photon crosses the disk, the brighter it is painted at the end of the simulation. The disk is also modelled as non-rotating. It is worth noting, however, that the redshift experienced by a photon travelling towards the disk could be computed from the geodesic integration, and by inverting this relation one could recover the redshift of the photons that would have reached the observer, allowing for a more realistic colour rendering of the accretion disk emission.

The program is implemented in Python, using CuPy arrays to handle all data manipulation. CuPy is functionally equivalent to NumPy, mirroring its interface and syntax almost exactly, but executing operations on a GPU rather than a CPU.

A CPU is designed to handle a small number of complex tasks sequentially, with typically fewer than a hundred cores optimised for single-threaded performance. A GPU, on the other hand, has thousands of smaller cores that excel at executing the same instruction across large datasets in parallel. In the context of ray tracing this is a natural fit: every pixel corresponds to an independent photon trajectory, and all of them undergo the same integration procedure, reducing the total computation time by orders of magnitude with respect to a sequential CPU implementation.

Since CuPy requires a CUDA-compatible GPU that is not available on most consumer machines, the program was run on Google Colaboratory (Colab), a free cloud-based platform that provides access to a dedicated GPU without requiring any specialised local hardware.

For the complete source code and the generated images, please refer to `https://github.com/martadelgado-cloud/TFG_GR_Image_Rendering_of_a_SBH`.

IV. RESULTS

The simulations were performed for a black hole of mass $M = 1$ in geometric units, without loss of generality, as any other value of M would result in a uniform rescaling of all distances, leaving the geometry of the image unchanged. The outer boundary of the black hole is defined by the event horizon at $r = 2M$ (Section II B). The accretion disk extends from $6M$ to $18M$: the inner boundary is set at $r_{\mathrm{ISCO}} = 6M$ as obtained from the effective potential analysis in Sections II C and II D. The camera is placed at a distance of $50M$ and has a screen size of (2000×1750).

To verify that the trajectories were being computed correctly, we first defined a one-dimensional screen and plotted the photon paths directly, following the example of Fig. 10 in [6], where a similar visualization is used to illustrate the null geodesic structure around a Reissner-Nordström black hole.

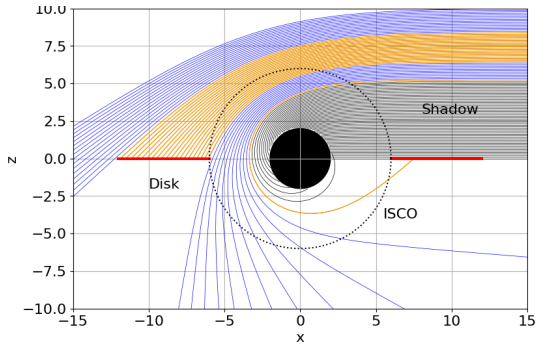

FIG. 3: One-dimensional representation of photon trajectories around a Schwarzschild black hole.

Note that an optically thick disk model was used here for visual clarity.

The different dynamical regions around a neutral, non-rotating black hole are clearly identifiable. Black paths correspond to photons that have fallen into the black hole, defining the shadow region. At its boundary, the yellow path corresponds to a photon with impact parameter $b \gtrsim b_c = 3\sqrt{3}\,M$: it passes arbitrarily close to the photon sphere at $r \approx 3M$ without falling in, eventually colliding with the underside of the accretion disk. Photons reaching the disk between $6M$ and $18M$ are also painted yellow, while blue paths correspond to photons that escape to infinity without intersecting any matter.

Having validated the code, we performed a full two-dimensional simulation at a viewing angle of 0.25 rad.

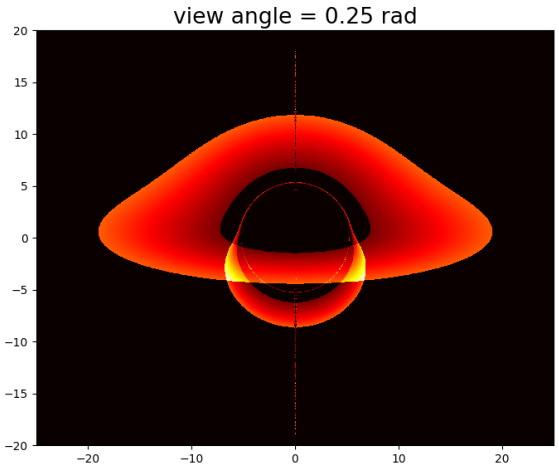

FIG. 4: First two-dimensional image rendering of a Schwarzschild black hole.

The overall result, shown in Fig. 4, is consistent with images produced by standard ray-tracing methods. However, unphysical values appear along the z-axis. This anomalous behaviour does not arise from discontinuities in the integration, but from numerical instability of the integrator in that region. Reducing the affine step $d\lambda$ resolves the problem at the cost of increased computation time. The fix was implemented by integrating the full screen at the standard step size, then reintegrating the problematic region with a step ten times smaller.

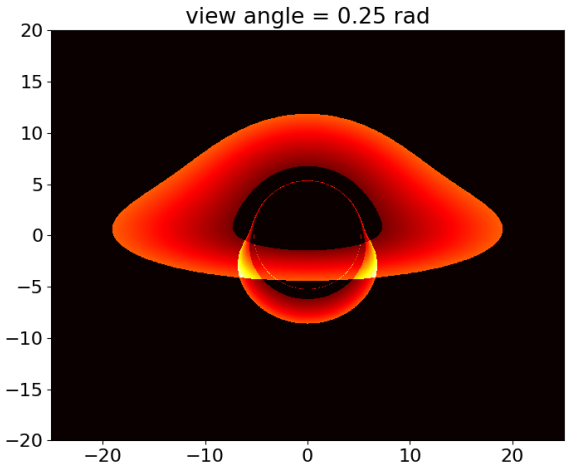

FIG. 5: Corrected two-dimensional image at viewing angle 0.25 rad.

The different regions visible in Fig. 5 can be identified as follows. As illustrated by Fig. 3, the large dark central region corresponds to the black hole shadow, where all photons fall into the event horizon. The bright ring delimiting it marks the shadow boundary, where photons pass arbitrarily close to the photon sphere before reaching the disk. The two broad orange-red lobes above and below the shadow are the direct and lensed images of the accretion disk: the upper lobe is the direct image, while the lower, more distorted lobe arises from photons that have been strongly deflected by the gravitational field, wrapping around the black hole before hitting the disk from below. The brightness gradient reflects the number of disk crossings, with the brightest region near the centre corresponding to photons that have orbited close to the photon sphere and accumulated the most crossings.

To conclude, the two limiting viewing angles were also simulated: an edge-on view at $\theta_{\text{obs}} = 0$ and a face-on view at $\theta_{\text{obs}} = \pi/2 \approx 1.57\,\text{rad}$, shown in Figs. 6 and 7 respectively.

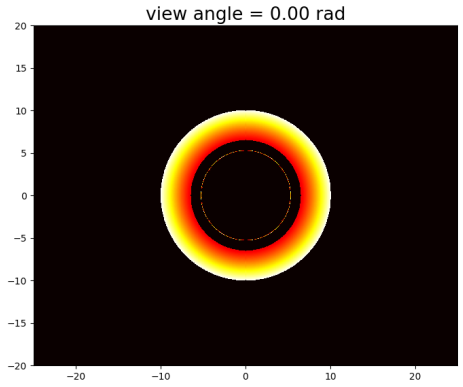

FIG. 6: Simulated image for an edge-on observer ($\theta_{\rm obs} = 0$).

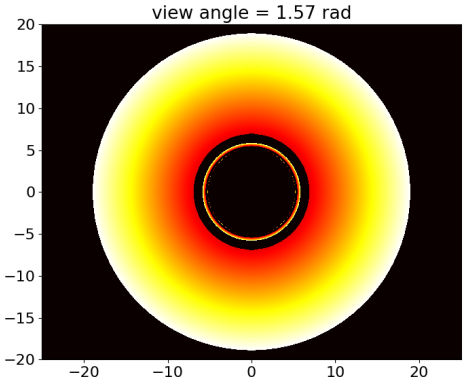

FIG. 7: Simulated image for a face-on observer ($\theta_{\rm obs} = \pi/2 \approx 1.57\,\text{rad}$).

The most notable difference between the two images is the apparent extent of the accretion disk. For $\theta_{\rm obs} = \pi/2$, the observer looks directly down onto the disk plane and the full radial extent is visible, producing a broad, bright annulus. For $\theta_{\rm obs} = 0$, the line of sight is tangential to the disk plane and the disk appears as a much narrower ring, with the outer regions at $r \sim 18M$ barely distinguishable from the background.

V. CONCLUSIONS

In this work we have successfully implemented a general-relativistic ray tracing code capable of rendering images of a Schwarzschild black hole surrounded by a geometrically and optically thin accretion disk. The null geodesic equations were integrated numerically using a 4th-order Runge-Kutta integrator, and GPU parallelisation via CuPy reduced the computation time by orders of magnitude with respect to a sequential CPU implementation.

The simulated images reproduce the characteristic features of the Schwarzschild spacetime, in agreement with those derived analytically through the effective potential analysis: the black hole shadow at $b_c = 3\sqrt{3}\,M$, the bright photon ring at $r = 3M$, and the direct and lensed images of the accretion disk extending from $r_{\rm ISCO} = 6M$ to $18M$.

A numerical instability along the polar axis was identified and corrected by applying a finer integration step in the affected region.

Future extensions of this work could proceed in several directions. Within the Schwarzschild spacetime, a more realistic accretion disk model could be incorporated: accounting for disk rotation would allow the gravitational and Doppler redshift of photons to be computed along each geodesic and mapped to a physical colour rendering of the disk emission. A natural generalisation would be the extension to the Kerr metric, which introduces black hole rotation and breaks the left-right symmetry of the image. Finally, adding a background radiation field would allow the simulation to render not only the disk emission but also the distortion of the surrounding sky by gravitational lensing.

Acknowledgments

First and foremost, I am deeply grateful to my supervisor, Dr. Luna, for offering me the opportunity to work with him and for his guidance throughout this project. I am also grateful to the future Dr. Climent for her support and companionship at every stage of this work. Finally, I wish to thank my family and friends for standing by my side from the very beginning of my degree through to the completion of this thesis.

[1] Event Horizon Telescope Collaboration, The Astrophysical Journal Letters **875**, L1 (2019), 1906.11238.
[2] Event Horizon Telescope Collaboration, The Astrophysical Journal Letters **930**, L12 (2022), 2311.08680.
[3] J. B. Hartle, *Gravity: An Introduction to Einstein's General Relativity* (Addison-Wesley, 2003), ISBN 9780805386622.
[4] G. D. Birkhoff, *Relativity and Modern Physics* (Harvard University Press, Cambridge, MA, 1923).
[5] W. H. Press, S. A. Teukolsky, W. T. Vetterling, and B. P. Flannery, *Numerical Recipes: The Art of Scientific Computing* (Cambridge University Press, 2007), 3rd ed., ISBN 9780521880688.
[6] Y. Kumaran and A. Övgün, Symmetry **14**, 2054 (2022), 2210.00468.

Generació d'Imatges en Relativitat General d'un Forat Negre

Author: Marta Delgado Vila, mdelgavi36@alumnes.ub.edu
Facultat de Física, Universitat de Barcelona, Diagonal 645, 08028 Barcelona, Spain.

Advisor: Raimon Luna i Perelló, raimonluna@icc.ub.edu

Resum: En aquest treball es presenta una simulació de *ray tracing* en relativitat general d'un forat negre de Schwarzschild envoltat per un disc d'acreció geomètricament i òpticament prim. Les trajectòries dels fotons es calculen mitjançant la integració numèrica de les geodèsiques nul·les usant un integrador de Runge-Kutta d'ordre 4, implementat en Python amb paral·lelització en GPU mitjançant CuPy. Les imatges resultants reprodueixen les característiques principals de l'espaitemps de Schwarzschild: l'ombra del forat negre, l'anell de fotons i les imatges directa i deflectada del disc d'acreció. Les simulacions es realitzen per a diversos angles d'observació, il·lustrant com la morfologia projectada del disc varia amb l'angle d'observació.
Paraules clau: Forat negre de Schwarzschild, *ray tracing*, geodèsiques nul·les, Runge-Kutta, disc d'acreció, lent gravitacional.
ODSs: Aquest TFG està relacionat amb els Objectius de Desenvolupament Sostenible 4 i 9.

Objectius de Desenvolupament Sostenible (ODSs o SDGs)

1. Fi de la es desigualtats		10. Reducció de les desigualtats	
2. Fam zero		11. Ciutats i comunitats sostenibles	
3. Salut i benestar		12. Consum i producció responsables	
4. Educació de qualitat	X	13. Acció climàtica	
5. Igualtat de gènere		14. Vida submarina	
6. Aigua neta i sanejament		15. Vida terrestre	
7. Energia neta i sostenible		16. Pau, justícia i institucions sòlides	
8. Treball digne i creixement econòmic		17. Aliança pels objectius	
9. Indústria, innovació, infraestructures	X		

El contingut d'aquest TFG, part d'un grau universitari de Física, es relaciona amb l'ODS 4 (Educació de Qualitat), i en particular amb la fita 4.4, ja que contribueix a la formació en física teòrica i computacional a nivell universitari. També es relaciona amb l'ODS 9 (Indústria, Innovació i Infraestructures), i en particular amb la fita 9.5, ja que desenvolupa eines de simulació numèrica que poden ser la base de futures aplicacions en astrofísica computacional.

Appendix A: Simulated images for all viewing angles

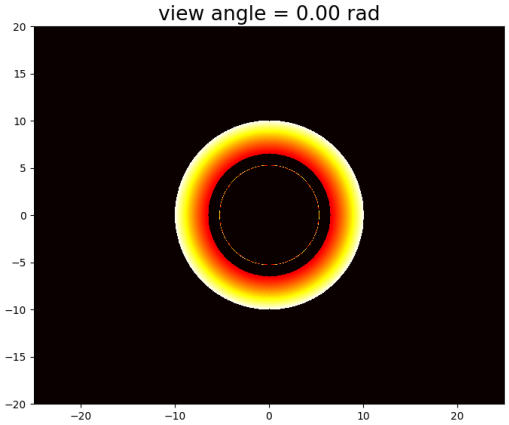

FIG. 8

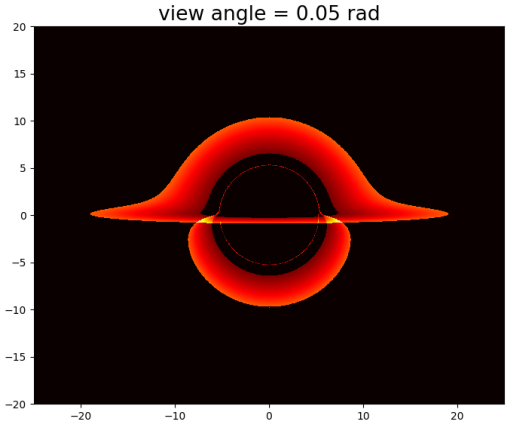

FIG. 9

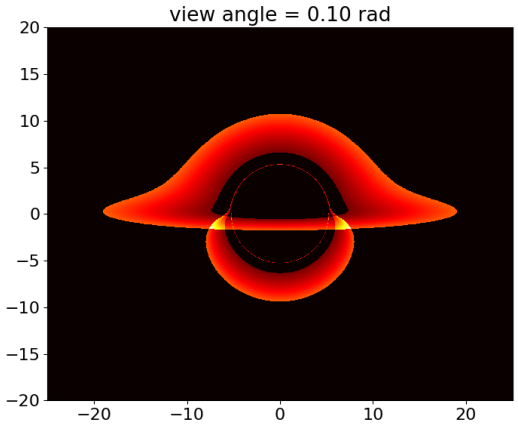

FIG. 10

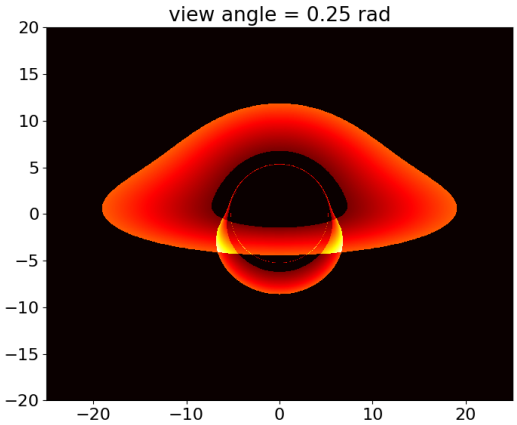

FIG. 11

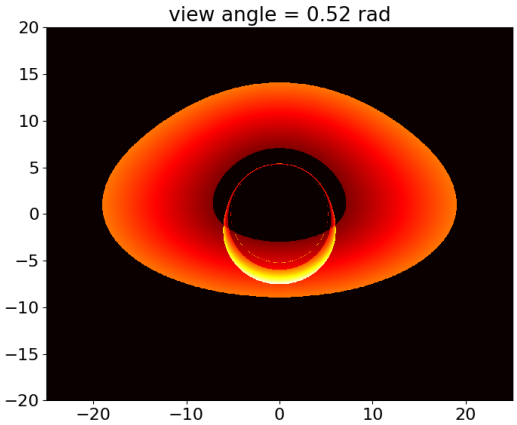

FIG. 12

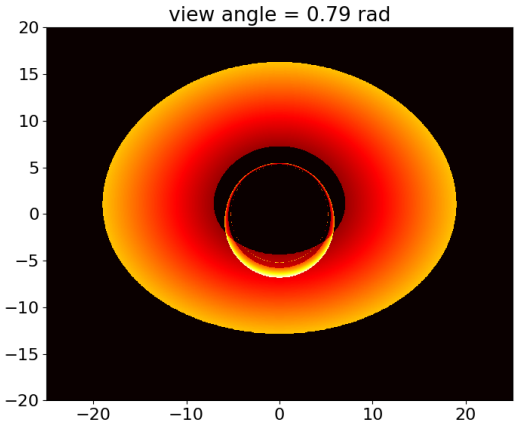

FIG. 13

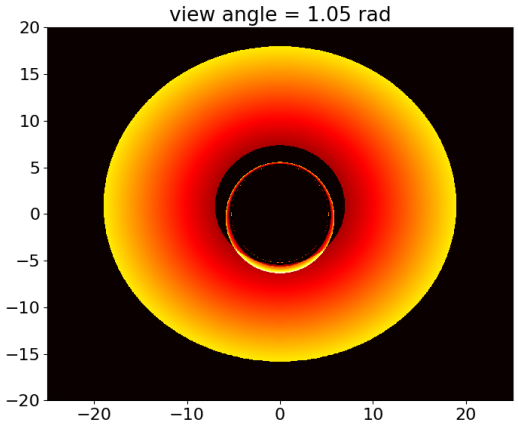

FIG. 14

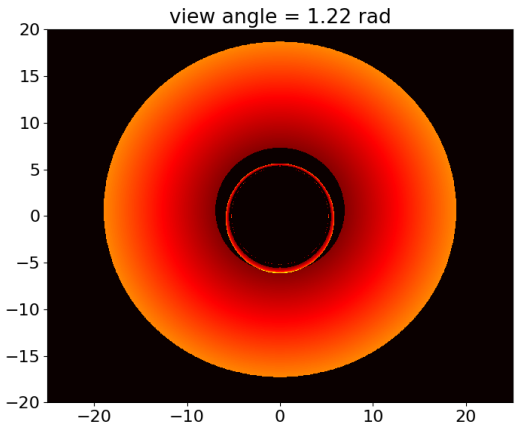

FIG. 15

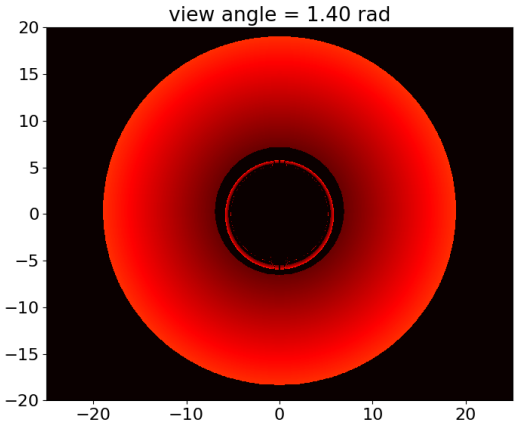

FIG. 16

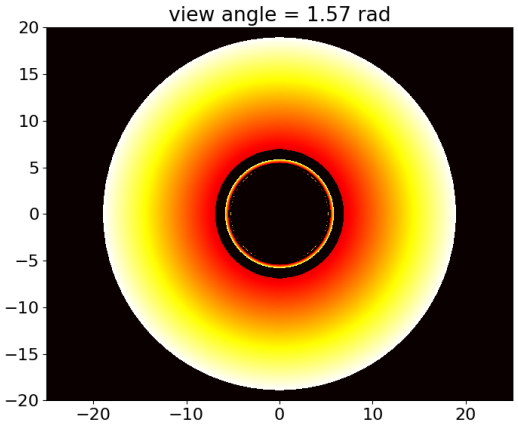

FIG. 17